A Novel Actin-Related Protein Is Associated with Daughter Cell Formation in *Toxoplasma gondii*[▽][†]

Jennifer L. Gordon, Wandy L. Beatty, and L. David Sibley*

Department of Molecular Microbiology, Washington University School of Medicine, St. Louis, Missouri 63110

Cell division in *Toxoplasma gondii* occurs by an unusual budding mechanism termed endodyogeny, during which twin daughters are formed within the body of the mother cell. Cytokinesis begins with the coordinated assembly of the inner membrane complex (IMC), which surrounds the growing daughter cells. The IMC is compiled of both flattened membrane cisternae and subpellicular filaments composed of articulin-like proteins attached to underlying singlet microtubules. While proteins that comprise the elongating IMC have been described, little is known about its initial formation. Using *Toxoplasma* as a model system, we demonstrate that actin-like protein 1 (ALP1) is partially redistributed to the IMC at early stages in its formation. Immuno-electron microscopy localized ALP1 to a discrete region of the nuclear envelope, on transport vesicles, and on the nascent IMC of the daughter cells prior to the arrival of proteins such as IMC-1. The overexpression of ALP1 under the control of a strong constitutive promoter disrupted the formation of the daughter cell IMC, leading to delayed growth and defects in nuclear and apicoplast segregation. Collectively, these data suggest that ALP1 participates in the formation of daughter cell membranes during cell division in apicomplexan parasites.

Toxoplasma gondii, the causative agent of toxoplasmosis, is a widespread opportunistic pathogen capable of invading virtually all nucleated cells in its many warm-blooded hosts (41). *Toxoplasma* is a protozoan parasite belonging to the phylum *Apicomplexa*, which includes other pathogenic members such as *Plasmodium*, the cause of malaria; *Cryptosporidium*, an agent of diarrheal disease; and *Theileria*, which is responsible for lymphoproliferative disease in cattle. In addition to their medical and economical importance, apicomplexans reveal an array of complex and elegant biological processes, which differ dramatically from those of their mammalian host cells. For example, these protozoa divide by a closed nuclear mitosis that occurs simultaneously, yet separately, from an unusual form of cytokinesis (39). Unlike typical cell division, which results in both a mother and daughter cell, apicomplexan daughter cells consume the maternal cytoplasm as they develop, resulting in the budding of new daughter cells that leave behind a residual body (30). Given their obligate, intracellular lifestyles, this mechanism of cell division is optimized to allow host cell invasion until the last minute of daughter cell maturation.

Internal budding by apicomplexans can be divided into three forms: schizogony, endopolygeny, and endodyogeny (46). Schizogony occurs by multiple rounds of asynchronous DNA replication followed by asynchronous mitosis without cytokinesis. The nuclei are ushered to the plasma membrane, and upon the final mitosis, daughter cells bud simultaneously from the mother cell (46). Endopolygeny is similar to schizog-ony in involving multiple rounds of DNA replication; however, mitosis does not follow each replication cycle, leading to a large polyploid nucleus. Consequently, concerted nuclear divisions and daughter cell budding follow the completion of DNA replication (49). Finally, endodyogeny occurs with a single round of DNA replication, followed by single mitosis that occurs simultaneously with daughter budding. While *Toxoplasma* is capable of all three forms of cell division, it most commonly replicates by endodyogeny (18, 31).

Several studies previously described the steps in endodyogeny including key changes in nuclear morphology (33, 34) that signify DNA replication and mitosis as well as markers of cytokinesis that are involved in the assembly of daughter cells (18). Nuclear division follows the duplication of the Golgi apparatus and the division of the apicoplast, a remnant endo-symbiont that contains a plastid-like genome (46). Daughter cell formation commences with the growth of a new inner membrane complex (IMC), which normally lies just beneath the plasma membrane of the parasite. The IMC is made up of flattened vesicles that overlay a basket weave of filamentous proteins called the subpellicular network (29). The function of these proteins is poorly understood, but they are similar to articulins, specialized cytoskeletal components found in other protozoa such as the ciliates and the euglenids (19). To date, only three IMC proteins have been experimentally character-ized in *Toxoplasma* (14, 15, 25, 26), although the genome indicates that a much larger family of these proteins is present (www.ToxoDB.org) (23).

During division, the polarity of new daughter cells is defined by the formation of the conoid, a cone-shaped structure that functions as a microtubule-organizing center for a system of singlet microtubules (reviewed in reference 30). The conoid and subpellicular microtubules that emanate from the apical polar ring provide the scaffold for the construction of the daughter cell IMC (46). Growth of the IMC progresses poste-

* Corresponding author. Mailing address: Department of Molecular Microbiology, Washington University School of Medicine, 660 S. Euclid Ave., St. Louis, MO 63110. Phone: (314) 362-8873. Fax: (314) 286-0060. E-mail: sibley@borcim.wustl.edu.
† Supplemental material for this article may be found at http://ec.asm.org/.
▽ Published ahead of print on 11 April 2008.

riorly and is defined by a terminal ring made up of the membrane occupation recognition nexus protein 1 (MORN1) and a type XIV myosin (MyoC), which may function to cinch the cell into two, completing nuclear division and cytokinesis (14). Although myosin has been shown to be involved in cytokinesis (6), the role of actin is unclear, as cell division is not susceptible to compounds that perturb the actin cytoskeleton (8, 37).

Actin and actin-related proteins (Arps) belong to a superfamily that is characterized by an actin fold (35). Arps are placed into a hierarchy according to their relatedness to actin: Arp1 exhibits the highest level of amino acid conservation to actin, followed by Arp2, etc. Arps carry out a variety of biochemical and structural roles in the cell (35), including the translocation of cargo along microtubules (5, 36), actin polymerization (32), and chromatin/heterochromatin remodeling (20, 40, 48). Actin-like proteins have also been characterized in bacteria, where they are involved in maintaining cell structure and polarity as well as preserving fidelity in DNA segregation (both genomic and episomal) during bacterial cell division (2, 3).

Recently, we reported the presence of 8 to 10 actin-like proteins (ALPs) encoded by members of the phylum *Apicomplexa* including *Toxoplasma*, *Plasmodium*, *Cryptosporidium*, and *Theileria* (12). To provide for a unified naming convention, we have suggested the use of "Arps" for apicomplexan proteins that are clear homologues of those already defined in other systems, while ALPs refer to those that are thus far unique to apicomplexans (12). Among these proteins are conserved orthologues to the Arp1 family (a major component of the dynactin complex) and the Arp4 and Arp6 families (subunits of various chromatin/heterochromatin remodeling machinery). Surprisingly, apicomplexans lack Arp2 and Arp3, and little is known about the function of other conserved actin-like proteins in this phylum. Here, we investigated the highly conserved ALP1 protein, which is unique to the *Apicomplexa* (12).

MATERIALS AND METHODS

Cell culture. Parasites were grown in human foreskin fibroblast (HFF) monolayers for 48 h and allowed to egress completely before being serially passed into new monolayers. HFF cells were maintained in Dulbecco's modified Eagle's medium supplemented with 10% fetal bovine serum, 2 mM glutamine, 20 mM HEPES (pH 7.5), and 10 μg/ml gentamicin. Parasites were harvested and purified by filtration using 3-μm polycarbonate filters as previously described (31). Parasite strains used in this study include RH p30GFP-HDEL (16), ROP-GFP (47), and RH GFP 5S65T (21).

Cloning of *ALP1*. *ALP1* was amplified using gene-specific primers (see Table S1 in the supplemental material) from a full-length RH tachyzoite cDNA library and cloned into the commercial cloning vector pCR4Blunt-TOPO using the Zero Blunt TOPO PCR cloning kit (Invitrogen, Carlsbad, CA) to generate plasmid pCR4-UP-R7 and transformed into *Escherichia coli* strain XL1 Blue (Stratagene, La Jolla, CA). The insert was sequenced by BigDye cycle sequencing (ABI), and the resulting full-length cDNA sequence was submitted to the NCBI database.

Knockout constructs. A knockout plasmid (pALP1KO) (see Table S1 in the supplemental material) was constructed by flanking the *ble* selectable marker with 5′ and 3′ genomic *ALP1*-flanking regions, as described previously (28). Negative counterselection was provided by either yellow fluorescent protein (11) or thymidine kinase (10) cassettes to increase the probability of isolating double-homologous recombination events. Hemagglutinin epitope (HA9)-tagged ALP1 constructs (N-terminal and C-terminal tags, respectively) were cloned into both vectors pTetO7-SAG1 and pTetO7-SAG4, which encode tetracycline (Tet) conditional promoters of various strengths (27), to generate plasmids for regulatable expression (pTet07SAG1/4-ALPHA9) (see Table S1 in the supplemental material). The *cat* gene under the control of the *SAG1* promoter was amplified (see Table S1 in the supplemental material) and inserted into the SacII site of the

vector, and regulated clones were isolated by chloramphenicol selection (22). Knockouts were attempted using the pALP1KO construct described above.

Construction of GFP(2)-ALP1-expressing parasites. *ALP1* cDNA containing an N-terminal Ala linker (Ala$_{10}$) was amplified and cloned into the *Toxoplasma* cloning vector pTUB/Ble/SAG, which contains the α-tubulin (*TUB*) promoter (kindly provided by Dominique Soldati, University of Geneva) and the 3′ untranslated region of the *SAG1* gene (*SAG1*) flanking a phleomycin resistance cassette (*ble*). The Ala$_{10}$-ALP1 coding region replaced the *ble* sequence at the NsiI-PacI sites to generate vector pBS-TUB/A$_{10}$ALP1/SAG1 (see Table S1 in the supplemental material). Green fluorescent protein (GFP) was amplified from plasmid pEGFP-C1 (BD Biosciences, San Jose, CA) using primers that encoded 5′ PstI and 3′ NsiI sites (see Table S1 in the supplemental material), and tandem GFP tags [GFP(2)] were cloned in frame and upstream of the Ala$_{10}$-ALP1 coding sequence at the NsiI site, resulting in plasmid pGFP(2)-ALP1. This plasmid was further modified by the addition of a chloramphenicol acetyltransferase (*cat*) cassette (see Table S1 in the supplemental material), also under the control of the *TUB* promoter, at the SacII restriction site downstream of GFP(2)-*ALP1*. The final construct was designated pGFP(2)-ALP1-TCS, and stable transformants were selected using chloramphenicol as described previously (44), sorted for GFP fluorescence using a BD FACSCalibur dual-laser flow cytometer (BD Biosciences), and cloned by serial dilution into 96-well plates (BD Labware, Franklin Lakes, NJ) containing HFF monolayers.

A plasmid containing the IMC1 gene (GenBank accession number AAK39634) fused at the C terminus to two copies of tomato red fluorescent protein [Tomato(2)] and driven by flanking 5′ αTUB and 3′ *DHFR* genomic regions from *T. gondii* was kindly provided by Boris Striepen (University of Georgia, Athens, GA). The SacII fragment containing the IMC1-Tomato(2) fusion and surrounding flanking regions was excised from this plasmid by restriction digestion and inserted into pSAG1/Ble/Sag1 at the SacII site in the multiple cloning site. The resulting vector [pIMC1-Tomato(2)-SAG1/Ble/SAG1] was transfected into GFP(2)-ALP1-expressing parasites, and stable clones were isolated by phleomycin selection as described previously (28).

Overexpression studies. *ALP* containing a C-terminal HA9 tag was amplified and cloned into the NsiI-PacI sites of the *Toxoplasma* cloning vector pGRA1/LacZ/SAG1, replacing the LacZ sequence with *ALP1* to generate vector pBS-GRA1/ALP1-HA9/SAG1 (pGAHS) (see Table S1 in the supplemental material). This construct expresses ALP-HA9 under the strong constitutive *GRA1* promoter (28). Parasites were transfected with plasmid pGAHS by electroporation as described above. Electroporated parasites were inoculated onto coverslips seeded with host cell monolayers and allowed to invade for 1 h at 37°C. Coverslips were then rinsed repeatedly in 1× phosphate-buffered saline and returned to culture in complete medium for 24 h before being processed for immunofluorescence microscopy. Approximately 50 random fields were imaged from three to four coverslips in two separate experiments, and the number of parasites per vacuole in transfected versus nontransfected cells was determined.

Generation of ALP1-specific antibodies. For protein expression, *ALP1* was amplified from an RH tachyzoite cDNA library using PCR primers encoding amino acids 80 to 386 of the ALP1 protein (primer sequences are available upon request). The resulting product was digested and cloned into the NdeI and NotI restriction sites of the pET22b expression vector (Novagen, EMD Biosciences, San Diego, CA) to generate plasmid pET22b-TGG_8730 (see Table S1 in the supplemental material). Recombinant protein was expressed in *E. coli* BL21(pLysS) cells (Stratagene) and purified over Probond resin (Invitrogen, Carlsbad, CA) under denaturing conditions according to the manufacturer's recommendations. Purified protein was dialyzed in 10 mM EDTA and used for antibody production in rabbits (Covance Research Products, Inc., Denver, PA). Rabbit anti-ALP1 antibodies (catalog number MO257) were affinity purified as described previously (17) using recombinant ALP1 to elute specific antibodies and are referred to as rabbit anti-ALP1 polyclonal antisera. Preimmune sera from the same rabbit was used as a control throughout.

Development of bradyzoites. Tachyzoites of type II strain ME49 were propagated in HFF cells as described above. In vitro conversion to bradyzoites was induced by growth at pH 8.0 in 0% CO_2 as previously described (42, 43). Tachyzoites were detected using the stage-specific protein SAG1 detected with monoclonal antibody (mAb) DG52. Differentiation into bradyzoites was detected by the loss of SAG1 staining and the appearance of the bradyzoite-specific antigen BAG1 (also known as BAG5) using a mouse mAb (50), which was kindly provided by Lou Weiss (Albert Einstein College of Medicine, Bronx, NY).

Reverse transcription (RT)-PCR. Total RNAs were isolated by treatment with TRIzol reagent (Invitrogen) for 5 min at room temperature, followed by extraction with 20% chloroform and precipitation with 50% isopropanol. RNAs were resuspended in diethyl pyrocarbonate-treated, RNase-free water to a final concentration of 1 μg/μl. RNA from partially sporulated *T. gondii* oocyst RNA (0.5

μg/μl) was kindly provided by Jay Radke (Montana State University, Bozeman, MT). In all samples, gene-specific mRNAs were reverse transcribed using SuperScript II reverse transcriptase and RNase H (Invitrogen). cDNAs were amplified from the first-strand synthesis reaction using 0.5 μM gene-specific primers (see Table S1 in the supplemental material) and KlenTag LA polymerase (Sigma-Aldrich, St. Louis, MO).

Immunofluorescence microscopy. Parasites were stained as intracellular rosettes grown overnight in HFF cells seeded onto coverslips or as extracellular cells adhered to polylysine-coated coverslips. Samples were fixed in 4% formaldehyde and permeabilized in 0.25% Triton X-100 for 15 min. Primary antibodies were added to coverslips, followed by staining with the appropriate secondary antibodies (i.e., goat anti-rabbit or goat anti-mouse antibody) conjugated to the fluorophore Alexa 488 or Alexa 594 (Molecular Probes, Invitrogen). Samples were mounted in Vectashield with DAPI (4′,6′-diamidino-2-phenylindole) (Vector Laboratories, Burlingame, CA). Images were acquired both as wide-field images and as z series in 0.255-μm steps using an Axioskop 2 MOT Plus fluorescence microscope equipped with 100× 1.4-numerical-aperture apochromat lens, an Axiocam Mrm monochrome camera (Carl Zeiss Inc., Thornwood, NY). Images were deconvolved using the Axiovision v.4.2 software (Carl Zeiss Inc.) using the inverse-filter algorithm or the nearest-neighbor algorithm. Images were processed in Adobe Photoshop CS v.8.0 (Adobe Systems Inc., San Jose, CA) using linear adjustments for all channels. Some images were falsely colored for clarity and consistency (see Fig. 2). A list of antibodies used for localizing parasite proteins can be found in Table S2 in the supplemental material.

Live-cell time-lapse imaging. HFF cell monolayers grown on 35-mm glass microwell dishes (MatTek Cultureware, Ashland, MA) were inoculated with parasites expressing either GFP(2)-ALP1 alone or both GFP(2)-ALP1 and IMC1-Tomato(2) and grown for ~18 h. Dishes were rinsed in Ringer's medium (155 mM NaCl, 3 mM KCl, 2 mM CaCl$_2$, 1 mM MgCl$_2$, 3 mM NaH$_2$PO$_4$, 10 mM HEPES [pH 7.4], 10 mM glucose) and returned to Ringer's medium supplemented with 10% fetal bovine serum for imaging. Live-cell imaging was done with a heated aluminum stage insert with a digital temperature control unit (heating insert P with Tempcontrol 37-2; Zeiss) using a LSM 510 Meta laser scanning confocal microscope (Carl Zeiss Inc.) equipped with a 63× 1.4-numerical-aperture Zeiss Plan Apochromat oil objective. Line scans were averaged (n = 8) for increased resolution. For time-lapse analysis, images were scanned every 10 min (5% 488-nm laser strength and 3% 543-nm laser strength) using LSM 510 software. Individual images were processed with Adobe Photoshop using linear adjustments before being imported into QuickTime v.7.2.0 (Apple Inc., Cupertino, CA).

EM. For immunolocalization at the EM level, infected cells were fixed in 4% paraformaldehyde–0.05% glutaraldehyde (Polysciences Inc., Warrington, PA) in 100 mM PIPES [piperazine-N,N′-bis(2-ethanesulfonic acid)]–0.5 mM MgCl$_2$ (pH 7.2) for 1 h at 4°C. Samples were then embedded in 10% gelatin and infiltrated overnight with 2.3 M sucrose–20% polyvinyl pyrrolidone in PIPES-MgCl$_2$ at 4°C. Samples were trimmed, frozen in liquid nitrogen, and sectioned with a Leica Ultracut UCT cryoultramicrotome (Leica Microsystems Inc., Bannockburn, IL). To localize the GFP(2)-ALP1 fusion, sections were probed with rabbit anti-GFP ab6556 antibody (Abcam Inc., Cambridge, MA), followed by 18-nm colloidal gold-conjugated goat anti-rabbit antibody (Jackson ImmunoResearch, West Grove, PA). To detect endoplasmic reticulum (ER) staining in association with ALP1, protein disulfide isomerase (PDI) was labeled with mAb SPA-891 (Stressgen; Assay Designs, Ann Arbor, MI) and 12-nm colloidal gold-conjugated goat anti-mouse antibody, and GFP-ALP1 was stained with rabbit anti-GFP ab6556 and 18-nm colloidal gold-conjugated goat anti-rabbit antibody. Parallel controls omitting the primary antibody were consistently negative. Sections were stained with 0.3% uranyl acetate–2% methyl cellulose and viewed on a Jeol 1200EX transmission electron microscope (Jeol USA Inc., Peabody, MA). For costaining of GFP-ALP and IMC-Tomato(2), the GFP tag was detected with goat anti-GFP ab5450 antibody (Abcam, Inc.), followed by 18-nm colloidal gold-conjugated donkey anti-goat antibody, and the red fluorescent protein (RFP) fusion was labeled with rabbit anti-RFP (Chemicon International Inc., Temecula, CA), followed by 12-nm colloidal gold-conjugated donkey anti-rabbit antibody (Jackson ImmunoResearch).

Western blot analysis. Parasite lysates were resuspended in sample buffer, electrophoresed on 10% sodium dodecyl sulfate-polyacrylamide gels, and transferred onto nitrocellulose using a Mini Trans-Blot electrophoretic transfer cell (Bio-Rad Laboratories, Hercules, CA) according to the manufacturer's recommendations. Secondary antibodies conjugated to horseradish peroxidase (Jackson ImmunoResearch Laboratories) were used for detection in combination with ECL Plus (Amersham Biosciences, Piscataway, NJ). Signals were detected using a Fuji FLA5000 phosphorimager and ImageGuage V4.22 (Fuji Film Medical Systems USA, Stamford, CT).

Nucleotide sequence accession number. The full-length cDNA sequence of *ALP1* was submitted to the GenBank database under accession number AAW23163.

RESULTS

ALP1 is conserved and constitutively expressed. The life cycle of *Toxoplasma* involves three distinct invasive stages known as tachyzoites (acute phase), bradyzoites (chronic phase), and sporozoites (environmental transmission) (9). We examined the expression of ALP1 by RT-PCR and compared it to actin (TgACT1), which is a constitutively expressed gene, versus several stage-specific controls. ALP1 was expressed in all three invasive stages, similar to TgACT1 (Fig. 1A). While the ALP1 signal appeared to be higher than that of actin, this likely reflects the efficiency of the primers used rather than the abundance of transcripts. Support for this conclusion is provided by the frequency of transcripts among randomly sequenced cDNAs, 50 expressed sequence tags (ESTs) correspond to TgACT1, while only 6 ESTs were found for ALP1 in *Toxoplasma* strain ME49 (http://www.ToxoDB.org). For further analysis, we generated ALP1-specific polyclonal antibodies to purified recombinant ALP1 expressed in bacteria. These antibodies recognized a single band of ~50 kDa in parasite lysates, consistent with the predicted molecular weight of ALP1 (Fig. 1B). Cross-reaction with host cell proteins was not detected (Fig. 1C). Despite similarity between ALP1 and TgACT1, antibodies to ALP1 recognized only recombinant ALP1 (rALP1) and anti-TgACT1 antibodies reacted only to recombinant TgACT1 (rTgACT1) (Fig. 1B). Anti-ALP1 antibodies stained both tachyzoites (detected with mAb DG52 against the surface antigen SAG1) and bradyzoites (detected with mouse mAb anti-BAG1) (50) equally well (Fig. 1C), indicating that it is expressed and likely functional in both of these stages. The images collected here were obtained from in vitro-cultured bradyzoites under conditions where >95% of vacuoles were BAG1$^+$ and SAG1$^-$. While these results support the idea that ALP1 is expressed in bradyzoites, we have not examined mature brain cysts for the expression of ALP1. We were unable to confirm sporozoite staining due to the lack of suitable material for immunofluorescence studies.

ALP1 is localized in distinct foci in a novel pattern. Location is often indicative of Arp function; for example, Arp4 to Arp11 are localized to the nucleus, while Arp1 to Arp3 are cytosolic (35). Consequently, we examined the location of endogenous ALP1 in comparison to several characterized cellular compartments in the parasite including the nucleus, plasma membrane, ER, cytoskeletal components, acidocalcisomes, and specialized apical secretory organelles (Fig. 2) (antibodies are listed in Table S2 in the supplemental material). Images were collected by wide-field microscopy and deconvolved to improve spatial resolution. ALP1 demonstrated a unique, punctate staining pattern (Fig. 2) that appeared scattered throughout the parasite cytosol. The pattern of ALP1 did not colocalize with antibodies specific to proteins found in the secretory compartments (micronemes [MIC2], dense granules [GRA1], rhoptries [ROP1-GFP], and ER [p30GFP-HDEL]) (Fig. 2). Importantly, ALP1 did not colocalize with the parasite's nucleus (HMGB-1) (Fig. 2), signifying that ALP1 probably does not carry out functions similar to those of Arp4 or Arp6. ALP1 staining did not colocalize with acidocalcisomes in the parasite,
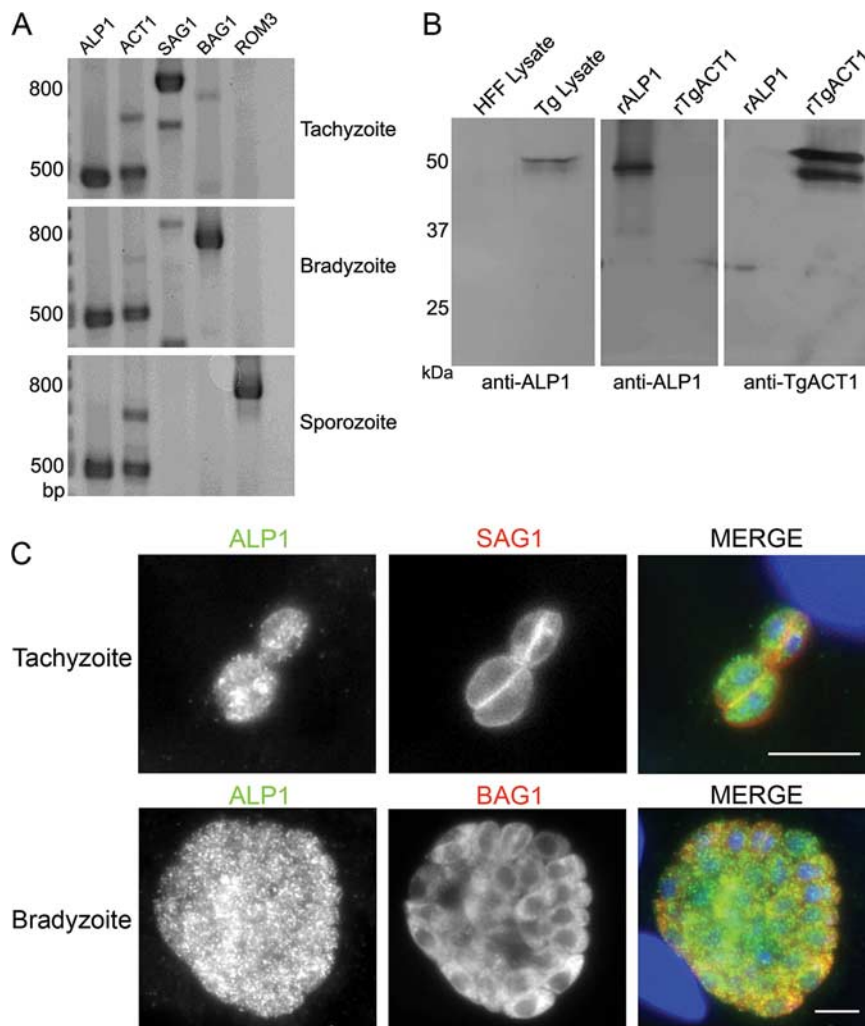
FIG. 1. ALP1 is a conserved protein that is expressed in multiple stages of the *Toxoplasma* life cycle. (A) RT-PCR experiments demonstrated that ALP1 was transcribed in the tachyzoite, bradyzoite, and sporozoite stages of the parasite's life cycle. ALP1 and TgACT1 were loaded at twice the amount loaded for controls. The stage-specific genes *SAG1* (tachyzoite surface antigen 1), *BAG1* (bradyzoite antigen 1), and *ROM3* (rhomboid protease 3) were used as controls. The presence of residual *SAG1* transcripts in bradyzoites was due to remaining tachyzoites after in vitro cyst conversion. (B) Anti-ALP1 rabbit polyclonal antisera reacted to a single band in parasite lysate (Tg Lysate) and to recombinant ALP1 (rALP1) but did not cross-react with the host (HFF) lysate or recombinant actin (rTgACT1). Similarly, rabbit polyclonal antisera raised against TgACT1 (anti-TgACT1) did not cross-react with rALP1. The smaller band in rTgACT1 is a breakdown product of the purified protein. (C) The ALP1 protein was expressed in both the tachyzoite and bradyzoite stages of *Toxoplasma*. Intracellular tachyzoites were stained for ALP1 using rabbit anti-ALP1 followed by secondary antibodies conjugated to Alexa 488 (green) and the stage-specific surface marker SAG1, detected using mouse mAb DG52, and secondary antibody conjugated to Alexa 594 (red). Bradyzoites were stained with rabbit-anti-ALP1 as described above (green) and the cyst antigen BAG1 using a mouse mAb, followed by secondary antibodies conjugated to Alexa 594 (red). DNA was stained with DAPI (blue). Scale bars, 5 μm.

as detected by staining for vacuolar H-ATPase (Fig. 2) and TgVPPase (data not shown). Furthermore, ALP1 did not co-localize with the subpellicular microtubules (TUB), suggesting that its role is also distinct from that of Arp1 (Fig. 2).

ALP1 associates with daughter cells during cell division. To gain further insight into the function of ALP1, tandem GFP tags [GFP(2)] were engineered at the N terminus, and the resulting construct was transfected into wild-type parasites. GFP(2)-ALP1-expressing parasites demonstrated the same staining pattern as wild-type parasites by immunofluorescence, although it was somewhat more diffuse (Fig. 3A). This pattern was similar using rabbit anti-ALP1, antisera to GFP, or the endogenous fluorescence of GFP (data not shown). Western

blot analysis comparing lysates of freshly egressed parasites expressing GFP(2)-ALP1 showed that the fusion was stable and underwent only minimal degradation (Fig. 3B). The expression level of the GFP-tagged ALP1 was comparable to that of endogenous protein, indicating that transgenic parasites overexpress ALP1 by about twofold, with no detrimental effects on grow rate or cell division (data not shown). Initial observations of GFP(2)-ALP1 in live cells revealed a similar diffuse staining pattern in nondividing cells (data not shown). In contrast, ALP1 was found in prominent clusters at the apical end of daughter cell IMCs in dividing cells (Fig. 3C).

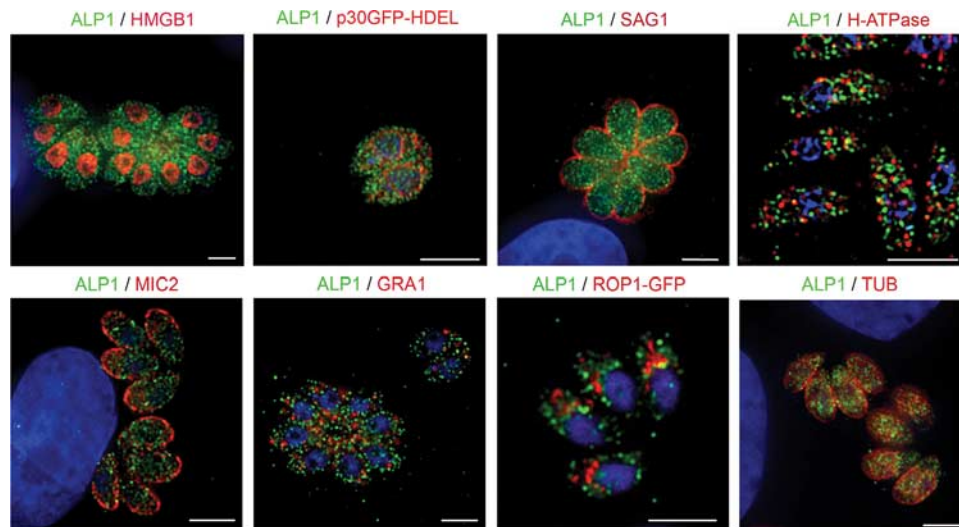To further examine the association with the newly formed IMC, the distributions of wild-type and tagged ALP1 were

FIG. 2. ALP1 does not localize to previously defined compartments in *Toxoplasma*. Parasites were stained with antibodies to proteins found in different subcellular compartments in *Toxoplasma*, including HMGB1 in the nucleus, p30-GFP-HDEL in the ER, SAG1 in the plasma membrane, H-ATPase in acidocalcisomes, MIC2 in micronemes, GRA1 in dense granules, ROP1-GFP in rhoptries, and TUB in microtubules (see Table S2 in the supplemental material). Images were acquired as *z* series and deconvolved using the inverse filter or nearest-neighbor algorithm. A representative slice of each *z* series is shown. ALP1 was stained with rabbit anti-ALP1 followed by secondary antibodies and is shown in green, and the contrasting protein is in red. In the case of p30-GFP-HDEL and ROP1-GFP, gray-scale images were falsely colored (red) so that ALP1 could be consistently shown in green. Examples are from intracellular parasites except for acidocalcisomes (H-ATPase), which were stained in extracellular parasites due to high background on the host cell. Scale bars, 5 μm.

reexamined following the synchronous invasion of cells and culture overnight. Newly formed daughter cells were detected by staining IMC with mAb 45.15, kindly provided by Gary Ward, University of Vermont (18, 25), and ALP1 was detected with affinity-purified rabbit anti-ALP1. Endogenous ALP1 in wild-type cells was largely punctate, as described above; however, in dividing cells, it was also detected in association with daughter cells visible primarily at the junction of adjacent daughter cells (Fig. 4A, arrows). GFP(2)-ALP1 also showed punctate staining but demonstrated an increased association with the IMC of forming daughter cells (Fig. 4B, arrows). A similar pattern was detected for C-terminally-tagged ALP1-HA9 (Fig. 4C, arrows), indicting that this result is not due to the fusion of GFP to the N terminus of ALP1. Parasites expressing GFP alone did not show any colocalization with IMC1 (Fig. 4D). Collectively, these findings indicate that the majority of endogenous ALP1 is found in a punctate pattern and weakly associated with the IMC in forming daughter cells, while this association increases in cells that contain a second, tagged copy of ALP1.

To better define the timing of the ALP1 association with daughter cells, synchronously infected monolayers were stained with markers designated to reveal distinct stages of cell division based on nuclear morphology (33), apicoplast copy number (45), and IMC formation as detected by IMC1 staining. In stage 1, which corresponds to the G_1 phase of the cell cycle, the inner membrane complex surrounded the maternal cell, the nuclei were small and compact, and a single apicoplast was detected. ALP1 in these cells was dispersed evenly throughout the cytoplasm in punctate foci (stage 1) (Fig. 5). As parasites entered S phase, the apicoplast divided, and the nucleus became enlarged. Changes in both IMC1 and ALP1 were not apparent at this stage (data not shown). Daughter cells

became evident at the onset of mitosis (stage 2) (Fig. 5) when the nucleus was pulled into the forming IMC of each daughter. ALP1 was observed accumulating at the apex of forming daughters, where it colocalized with the IMC protein IMC1 (Fig. 5, arrows). Stages 3 and 4 exhibited a significant increase in the level of colocalization between ALP1 and IMC1 as the daughter IMCs elongated. The dividing nucleus was pulled further into the growing cells, illustrated by its "horseshoe" shape, until mitosis was completed (Fig. 5 [arrows depict the colocalization of ALP1 and IMC1]). Interestingly, the association of ALP1 and IMC1 was less apparent as daughter cells started to bud (stage 5) (Fig. 5), and ALP1 returned to its punctate appearance dispersed throughout the cytoplasm and the residual body.

Accumulation of GFP(2)-ALP1 on the daughter cells precedes IMC1. The IMC protein IMC1 is a major component of the subpellicular protein network that tightly apposes the cytoplasmic face of the IMC (25). IMC1 is one of the earliest known markers of daughter cell formation. Live-cell imaging of IMC tagged with fluorescent protein markers has helped to define the temporal connection between DNA replication and cytokinesis in *Toxoplasma* (18). To take advantage of this approach, we engineered our GFP(2)-ALP1-expressing parasite lines to also express an *IMC1* allele fused to a tandem dimer of the RFP Tomato, referred to as IMC1-Tomato(2).

Host cell monolayers were infected with transgenic *Toxoplasma* and grown 18 h prior to live confocal imaging. Parasite vacuoles undergoing cell division were imaged at 10-min intervals until daughter cells emerged from the mothers. Surprisingly, we observed that GFP(2)-ALP1 was present on daughter cells up to 20 min before IMC1-Tomato(2) became visible (Fig. 6, white arrows) (see the movie in the supplemental material). Once both proteins were evident, they remained
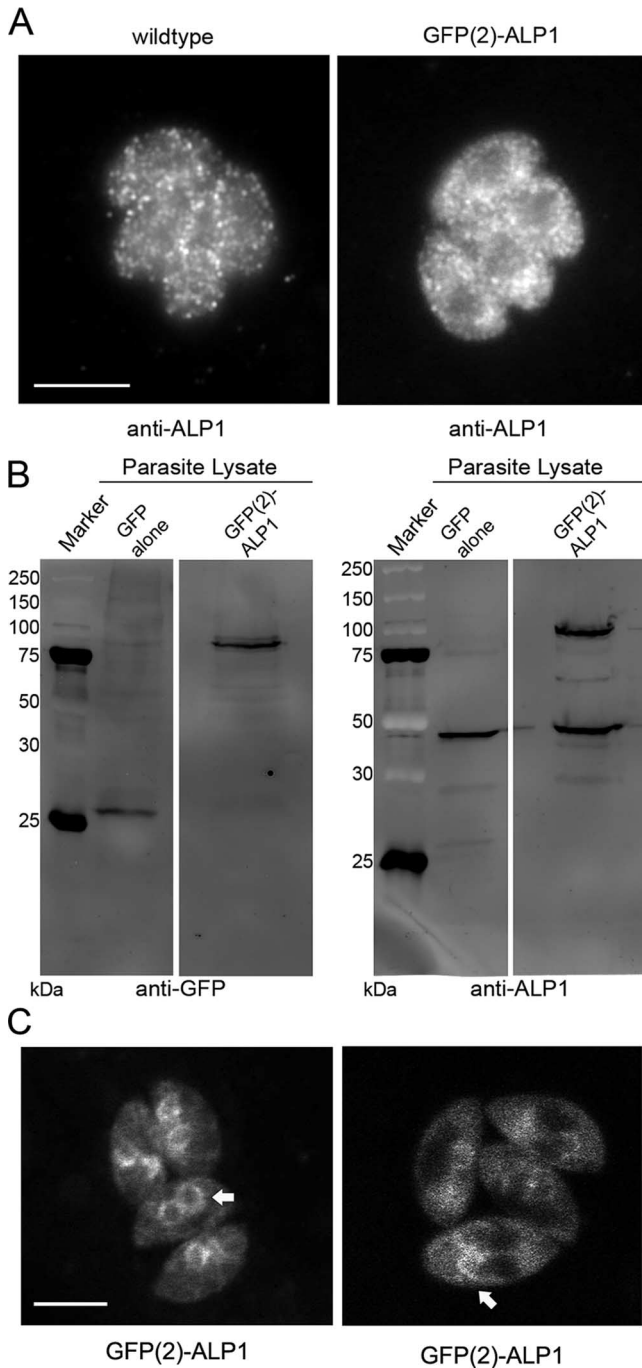
FIG. 3. Expression of a dual-GFP-tagged ALP1 construct [GFP(2)-ALP1] yields a stable protein with staining patterns similar to those of the endogenous protein. (A) GFP(2)-ALP1 exhibits a staining pattern similar to that of endogenous ALP1. The image was stained using rabbit anti-ALP1 antibodies followed by secondary antibodies conjugated to Alexa 488. Scale bar, 5 μm. (B) The recombinant GFP(2)-ALP1 protein expressed in wild-type parasites exhibited minimal degradation as detected in parasite lysates by Western blot assays using mouse mAb B34 (Molecular Probes) against GFP. Lysate from parasites expressing GFP alone was used as a control. The marker lane is indicated in kilodaltons. (C) Live-cell imaging of GFP(2)-ALP1 reveals a partial association with the forming daughter cells in dividing cells (arrows). Scale bar, 5 μm.
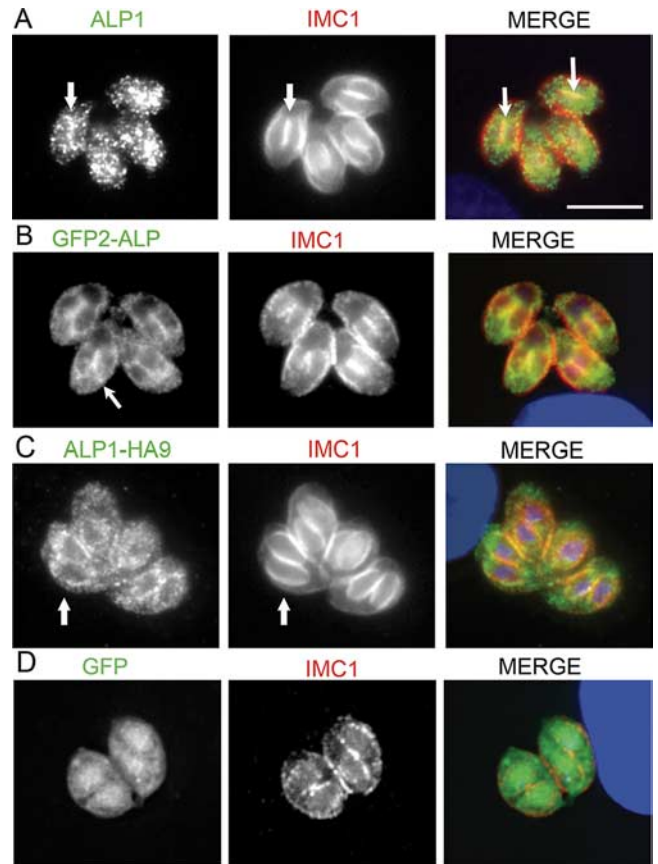

FIG. 4. Localization of ALP1 in dividing cells. (A) Endogenous ALP1 showed a predominantly punctate distribution with some accumulation at the junction of adjacent daughter cells (arrows). (B) Distribution of ALP1 in cells expressing GFP(2)-ALP1 was more prominently associated with daughter cells (arrows). (C) A similar punctate distribution with more apparent outlining of the daughter cells was detected in ALP1-HA9-expressing cells. Overlap with IMC1 is indicated by the arrows. In A to C, ALP1 was stained with affinity-purified rabbit anti-ALP1 polyclonal antisera followed by secondary antibodies conjugated to Alexa 488 (green). (D) In contrast, parasites expressing GFP alone did not demonstrate colocalization with nascent daughter cells. GFP (green) was imaged based on inherent fluorescence. In all panels, IMC1 was stained with mouse mAb 45.15 followed by secondary antibodies conjugated to Alexa 594 (red), and the nucleus and apicoplast (blue) were stained with DAPI. Scale bar, 5 μm.

colocalized for the duration of cell division (Fig. 6). These results confirm that ALP1 is associated with forming daughter cells, and it arrives there before the appearance of the IMC1 protein.

ALP1 associates with apical complexes of daughters early in cell division. During the cell division of *Toxoplasma*, the Golgi apparatus first divides, followed by the separation of the apicoplast, which is tied to the division of the centrioles (30, 31, 45, 46). The first indication of nascent daughter cells is the formation of an open, dome-shaped cap of membrane that overlies the daughter cell conoid, which appears as two slanted electron-dense flanges in cross section (39). Several parasite proteins were previously localized to early daughter cells, including IMC1, centrin 2, and MORN1 (46). To examine the association of ALP1 with early daughter cells, GFP(2)-ALP1-expressing parasites were analyzed by immuno-EM.
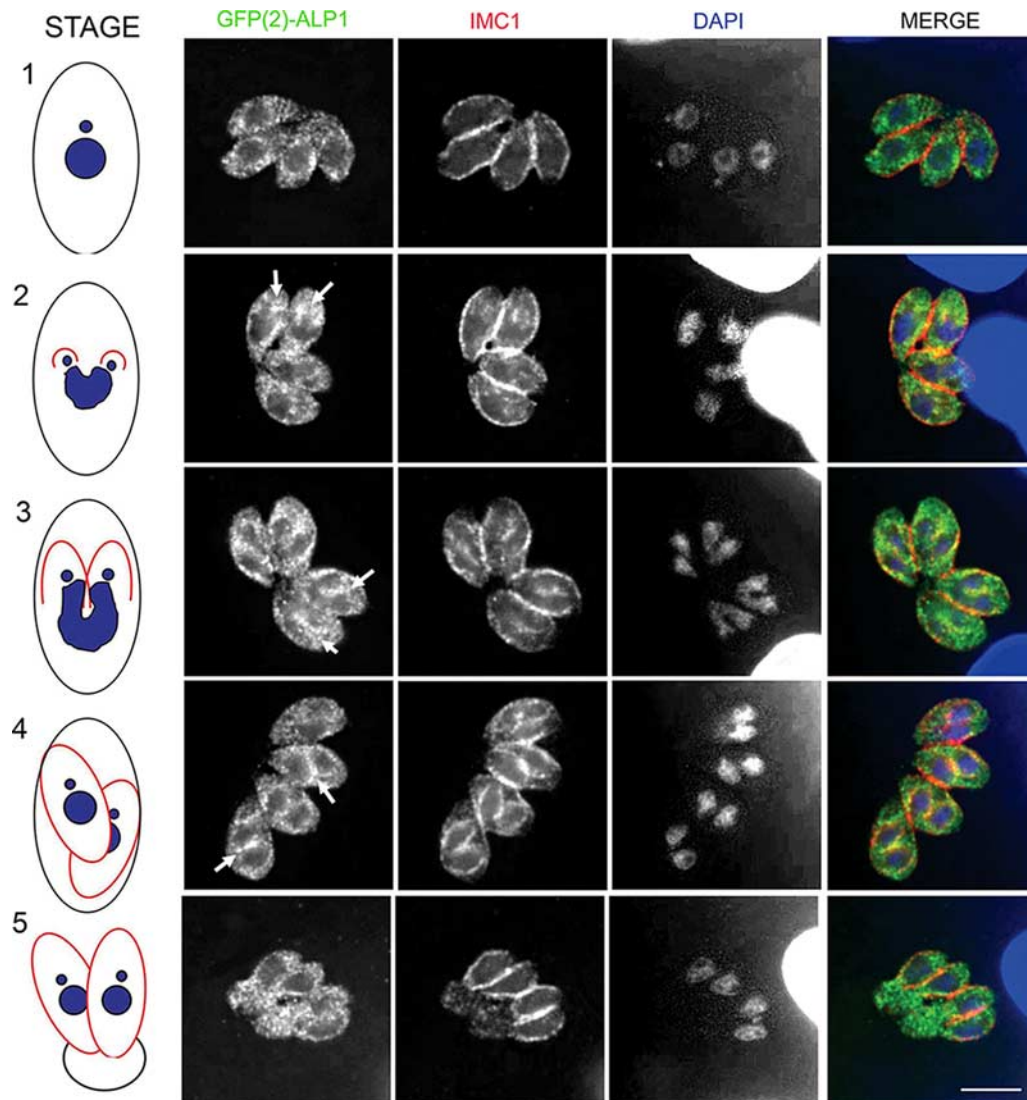
FIG. 5. ALP1 associates with newly forming daughter cells during cell division. GFP(2)-ALP1 demonstrated a partial association with forming daughter cells but was dispersed throughout the cytoplasm in budding and adult parasites. Arrows depict regions where ALP1 is concentrated in the vicinity of daughter cells as revealed by staining for IMC1. Characteristic stages of parasite cell cycle progression are diagrammed in the model to the left (see the text for explanation). Images were acquired as z series and deconvolved using the nearest-neighbor algorithm, and a representative slice of each z series is shown. GFP(2)-ALP1 was stained with rabbit anti-ALP1 polyclonal antisera followed by secondary antibodies conjugated to Alexa 488 (green); IMC1 was detected using mouse mAb 45.15 followed by secondary antibodies conjugated to Alexa 594 (red), and the nucleus (blue) was stained with DAPI. Scale bars, 5 μm.

Cryo-EM revealed a prominent staining of GFP(2)-ALP1 along a flattened system of membranes overlying the newly formed daughter conoids (Fig. 7). The membranes of newly formed daughter cells were readily recognizable based on their positioning outside the dividing maternal nucleus and directly above the conoid, which appears as two slanted white lines in cyro-EM (white asterisks in Fig. 7). Staining of GFP(2)-ALP1 was also detected on the membranes of elongated daughter cells, suggesting that ALP1 interacts with the IMC during growth. GFP(2)-ALP1 was also seen on membranous structures bridging the space between the mother nucleus (N) and the daughter as well as on the forming IMC (Fig. 7C). The localization of GFP(2)-ALP1 to the IMC was specific to the expression of the ALP1 fusion protein and was not seen in cells expressing GFP alone (Fig. 7D). To further examine the nature of these vesicles, cells were costained with antibodies to GFP(2)-ALP1 (detected with antibody to GFP and secondary antibodies conjugated to18-nm gold) and the ER marker PDI (detected with secondary antibodies conjugated to 12-nm gold). PDI was located in the nuclear envelope, which is continuous with the ER, as well as on transport vesicles between the nucleus and daughter cell IMC (Fig. 7E). GFP(2)-ALP1 was colocalized along these transport vesicles (Fig. 7E).

Time-lapse images presented in Fig. 6 suggest that ALP1 associates with the daughter cell prior to the arrival of IMC1. To examine this further, cryo-EM sections were doubly stained to detect exogenously expressed GFP(2)-ALP1 (18-nm gold) and IMC1-Tomato(2) (12 nm). GFP(2)-ALP1 was preferen-
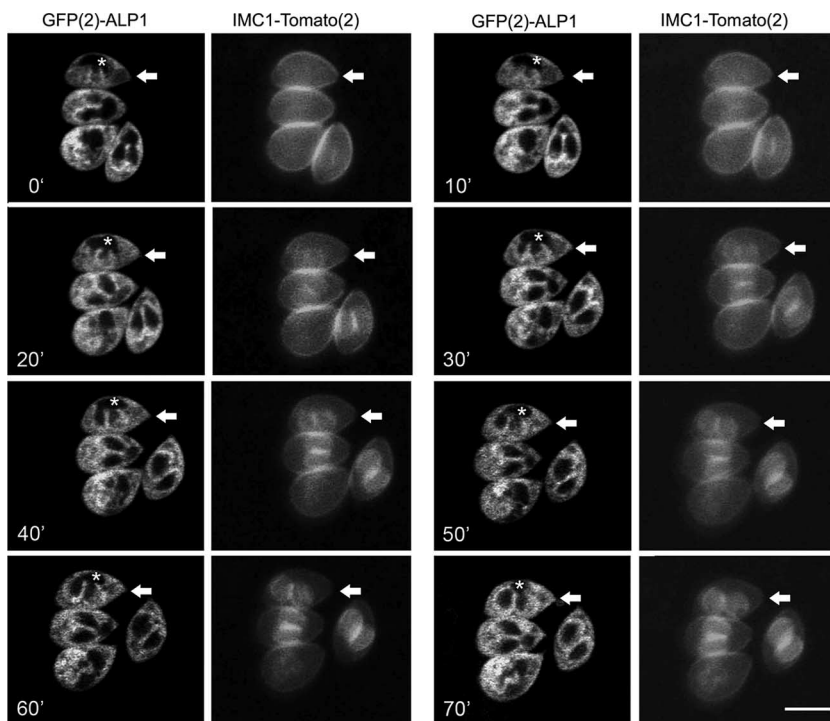
FIG. 6. Time-lapse analysis of *T. gondii* undergoing active cell division. GFP(2)-ALP1 was enriched on daughter cells prior to detection of IMC1-Tomato(2). Transgenic parasites expressing both GFP(2)-ALP1 and IMC1-Tomato(2) were imaged based on intrinsic fluorescence at 10-min intervals for 70 min (the time stamp in the lower left corner is given in minutes). White arrows draw attention to a cell that shows the accumulation of GFP(2)-ALP1 in the cupped structures of the daughters (indicated by an *) ~20 min before the appearance of IMC1-Tomato(2). See the movie in the supplemental material. Scale bar, 5 μm.

tially associated with immature daughter cell IMC membranes, as defined by limited IMC growth (Fig. 7F). At later stages, where the IMC of the daughter cells was more fully elongated and the host cell nucleus was drawn into the daughter cells, both GFP(2)-ALP1 and IMC1-Tomato(2) were detected along the membranes of the daughter cell (Fig. 7G). Collectively, these results indicate that the early daughter cell IMC is defined by a flattened system of membranes associated with the conoid, and ALP1 is recruited to the daughter cell IMC prior to the IMC1 protein.

ALP1 is essential for daughter IMC formation. Several genetic approaches were attempted in order to define the cellular function of ALP1. First, we attempted to disrupt the endogenous gene by allelic replacement combined with negative selection (see Materials and Methods). We were unable to obtain clones lacking the *ALP1* gene using this approach, indicating that its function was essential to parasite viability. We modified our strategy to utilize the conditional tetracycline-repressible system developed for *Toxoplasma* (27) (see Materials and Methods). While we could readily isolate parasites expressing regulatable *ALP1* alleles, it was not possible to obtain genomic knockouts in any of the assorted conditional backgrounds (data not shown). In transient transfections, the expression of ALP-HA9 driven by the pTetO7-SAG1 or pTetO7-SAG4 promoter revealed segregation and cell division defects in a number of cells (data not shown), suggesting that the level or timing of expression from these promoters was detrimental.

Since we were unable to disrupt *ALP1*, we instead overex-

pressed the protein with a C-terminal HA9 tag under the control of the strong constitutive promoter *GRA1* (4), which is estimated to be ~100 times stronger than *ALP1* based on EST frequencies (http://ToxoDB.org). Transient transfection under these conditions typically leads to cells expressing very different levels of protein due to differences in the plasmid copy number, which is expected to result in a range of levels of phenotypic expression. In cells that overexpressed ALP1 strongly, as judged by the intensity of staining, cell division was profoundly disrupted. *Toxoplasma* divides every 6 to 8 h by binary fission, and the number of parasites in a single vacuole is a direct reflection of this doubling time (33). The average number of parasites per vacuole was substantially lower in ALP1-overexpressing cells versus nonexpressing cells in the same culture (Fig. 8A). In ALP1 overexpressers that progressed beyond the two-cell stage, division was often asymmetric, with parasites being delayed in nuclear division (Fig. 8Bi). ALP1 overexpressers also showed asymmetric division, giving rise to odd numbers of parasites (Fig. 8A). In addition, ~40% of vacuoles contained mixed populations of ALP1 overexpressers and nonexpressing cells (Fig. 8Bii), suggesting that division was inhibited when ALP1 was overexpressed and that that the loss of the plasmid was strongly favored, allowing normal growth to resume. This result was not due to the instability or toxicity of GFP alone, as transgenic parasites stably retain this marker over many generations without loss (21; unpublished data).

To provide greater insight into the specific role of ALP1, overexpressing cells were examined to determine their nuclear
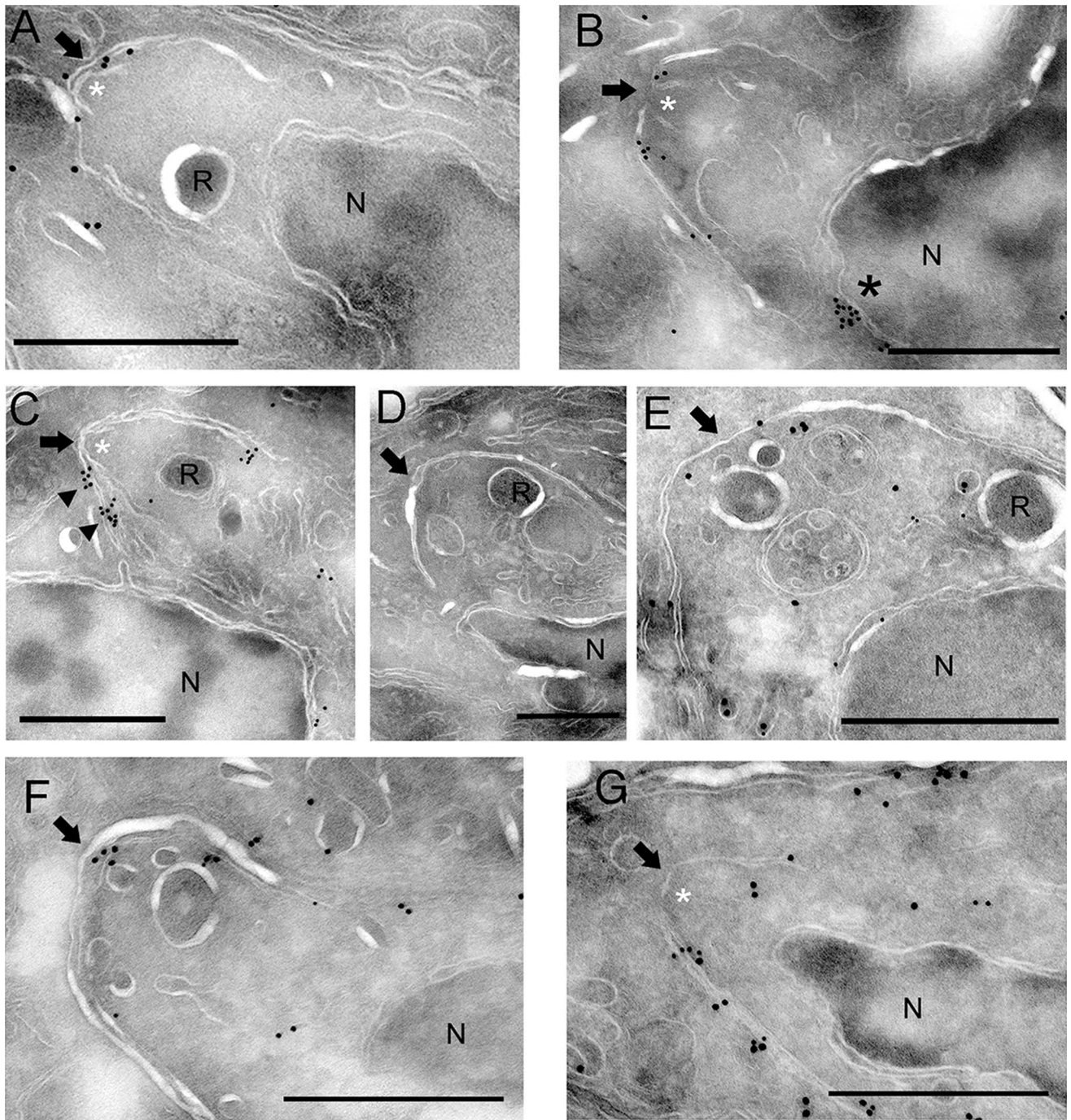
FIG. 7. GFP(2)-ALP1 is involved in early events of daughter cell formation. (A and B) GFP(2)-ALP1 localized to the membrane of the daughter cell IMC encompassing the newly formed conoid, a small cap-like structure seen just under the IMC membranes (white asterisks). ALP1 staining was also detected on the nuclear envelope (* in B). Images come from independent cells. (C) GFP(2)-ALP1 was enriched in membranous structures associated with the daughter IMC (arrowheads). (D) Staining of daughter cells was specific to GFP(2)-ALP1, shown by the absence of staining in control cells expressing GFP alone. GFP(2)-ALP1 (A to C) or GFP (D) was stained with rabbit anti-GFP antibody ab6556 (Abcam) and detected with secondary antibodies conjugated to 18-nm colloidal gold. (E) Costaining of ALP1-GFP (18-nm gold) and the ER marker PDI (12-nm gold). ALP1 was associated with ER-derived vesicles that lie between the maternal nucleus (N) and the daughter cell IMC (arrow). GFP(2)-ALP1 was stained with rabbit anti-GFP antibody ab6556 (Abcam) and detected with secondary antibodies conjugated to 18-nm colloidal gold. PDI was labeled with mAb SPA-891 (Stressgen; Assay Designs, Ann Arbor, MI) and 12-nm colloidal gold-conjugated goat anti-mouse antibody. (F) Costaining of GFP(2)-ALP (18-nm gold) shows deposition on the IMC membranes of early daughter cells prior to accumulation of IMC1-Tomato(2) (12 nm). (G) At later stages, both GFP(2)-ALP1 (18-nm gold) and IMC1-Tomato(2) (12 nm) were detected on the IMC membranes of the forming daughter cell. In F and G, GFP(2)-ALP1 was labeled with goat anti-GFP ab5450 (Abcam, Inc.) followed by 18-nm colloidal gold-conjugated donkey anti-goat, and IMC1-Tomato(2) was labeled with rabbit anti-RFP (Chemicon) followed by 12-nm colloidal gold-conjugated donkey anti-rabbit antibody (Jackson ImmunoResearch). The daughter prehoptry compartment (R) and the mother nucleus (N) are labeled for orientation. The arrow in each panel indicates the apex of the daughter cell IMC. Scale bar, 0.5 μm.
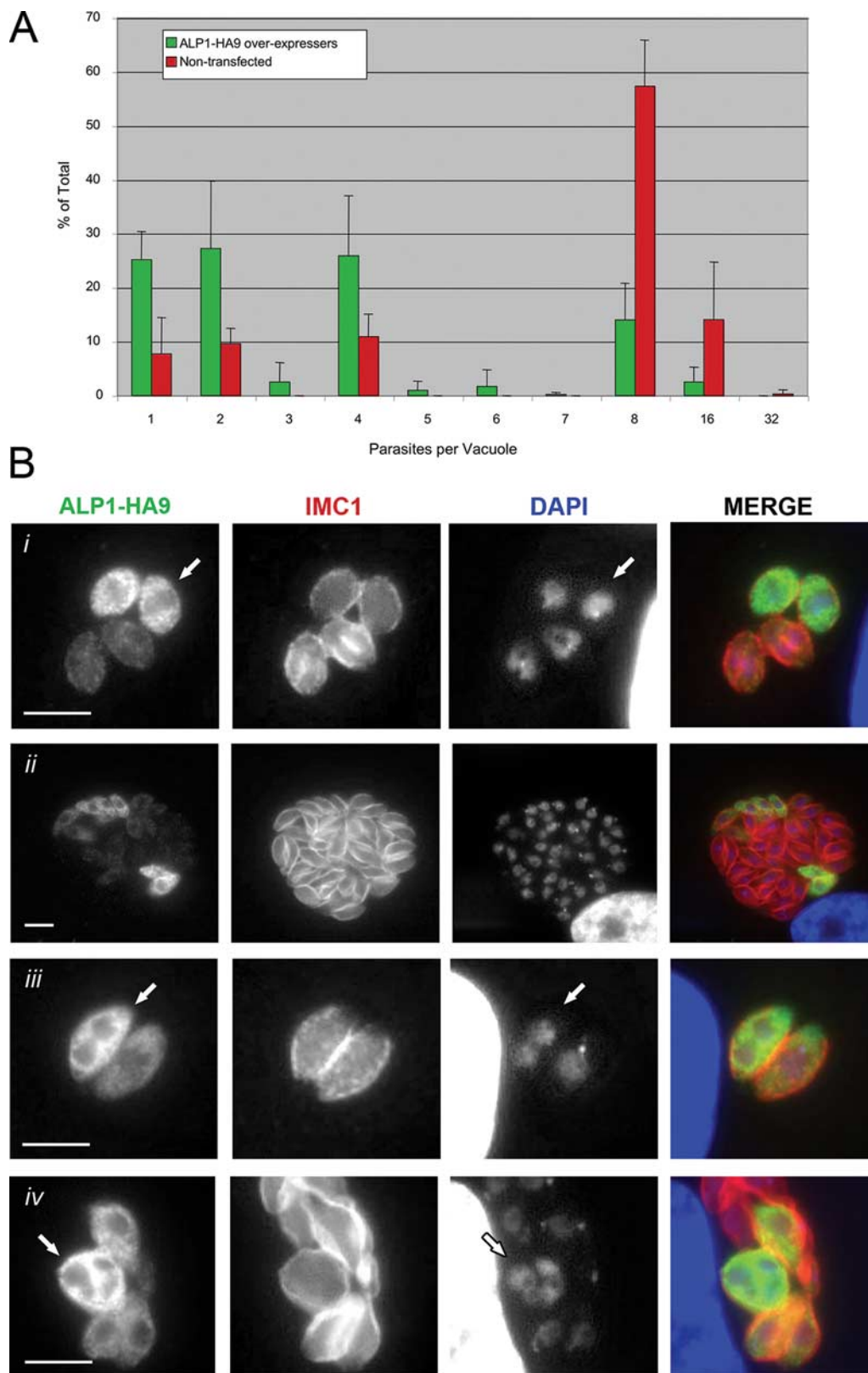
FIG. 8. Overexpression of ALP1-HA9 leads to replication defects. (A) ALP1-HA9-expressing parasites replicated slower than untransfected parasites, resulting in decreased numbers of parasites per vacuole at 24 h posttransfection. Counts are averaged from replicate samples (three to four) in two separate experiments. Green bars, ALP1-HA9-expressing vacuoles; red bars, nontransfected vacuoles. (B) Replication defects result from a delay in cell cycle progression and/or failure to initiate daughter cell formation. (i) Parasites that overexpress ALP1-HA9 (arrow) within a single vacuole were delayed in cell cycle progression compared to cells with low levels of expression, as seen by the horseshoe shape of the nucleus

and apicoplast contents as well as the stage of division as determined by IMC1 staining. Strikingly, ~25% of cells that overexpressed ALP1 failed to form daughter cell IMC structures, as revealed by the complete lack of IMC1 staining, while nuclear division and apicoplast division were unimpaired. Most commonly, this resulted in cells containing two nuclei and two apicoplasts yet not showing evidence of internal daughter cell formation (Fig. 8Biii), although occasional segregation defects of either the nucleus or apicoplast were noted (data not shown). Additionally, some cells underwent a second round of nuclear division without forming internal daughter cells, as shown by a lack of IMC1 staining and the formation of four distinct nuclei (Fig. 8Biv). Collectively, these results indicate that the overexpression of ALP1 results in the profound disruption of cell division due to the failure of the daughter IMCs to form.

DISCUSSION

Actin-like proteins play a variety of functions in eukaryotic cells including chromatin remodeling, vesicle transport, and controlling actin dynamics (35). ALP1 is an actin-like protein that is highly conserved among apicomplexans. ALP1 is also not distributed in a pattern that would be consistent with those of other known Arps such as microtubule-based transporters (i.e., Arp1) or nuclear Arps (i.e., Arp4 and Arp6), which have been defined in other systems but not yet studied in parasites. Instead, ALP1 was associated with the construction of the daughter cell IMC during endodyogeny in *Toxoplasma*. Collectively, our studies suggest that ALP1 likely plays a role in the unique form of cell division utilized by apicomplexan parasites.

Multiple phases of the *Toxoplasma* life cycle are devoted to asexual replication, a process that is important for the expansion of the parasite in various host cells. RT-PCR analysis showed that ALP1 was expressed in the tachyzoite, bradyzoite, and sporozoite stages of the *Toxoplasma* life cycle. Sporozoites themselves are growth arrested, but they must be prepared to initiate endodyogeny upon excystation and the subsequent invasion of host cells (9). Expression profiles provided by the *Plasmodium* genome database (www.plasmodb.org) (1) show that the ALP1 orthologue in *Plasmodium falciparum* (*P. falciparum* ALP1 [PfALP1] and AAN35700) (12) is upregulated in the erythrocytic stages as parasites move from the late trophozoite to the late schizont stage. This is consistent with a role of PfALP1 in daughter cell formation, as this is the stage in *P. falciparum* where parasites undergo schizogony. While we have not explored the specific ALP1 orthologues outside of *Toxoplasma*, the conservation of ALP1 among different apicomplexans suggests that they serve similar roles in these related organisms.

ALP1 was found primarily in small punctate structures in the cytosol that did not colocalize with known compartment markers. In separate studies, we have observed that ALP1 is part of a high-molecular-weight complex (J. L. Gordon, unpublished data), which may explain its predominant punctate pattern in immunofluorescence microscopy. While endogenous ALP1 is largely cytoplasmic and found in punctate clusters, it is also transiently associated with the IMC and implicated in the formation of daughter cells. The reason for the more prominent staining of daughter cell IMCs with epitope-tagged or GFP fusions with ALP1 is not clear but could relate to the approximately twofold-higher levels of expression than those of wild-type cells. This level of expression in the stable transgenic parasites did not appear to be deleterious. However, when strong constitutive promoters were used to drive much higher levels of expression in transiently transfected parasites, the overexpression of ALP1 disrupted daughter cell formation. These effects were independent of tagging at the N or C terminus but, rather, correlated with relative expression levels, suggesting that a tight control of ALP1 levels is important for its function. Collectively, these results indicate that ALP1 is transiently associated with the daughter cell IMCs and that slight overexpression shifts the equilibrium in favor of association, while strong overexpression disrupts the function of ALP1 and prevents daughter cell formation.

Live-cell imaging of GFP-tagged ALP1 was used to elucidate its cellular function in parasites undergoing cell division. We traced ALP1 during endodyogeny by immunofluorescence microscopy using key morphological changes in the parasite that distinguished each stage of the cell cycle. During G_1, ALP1 was localized in small, cytoplasmic foci that did not costain with proteins that marked various cellular compartments. However, at the onset of mitosis, the distribution of ALP1 changed to partially colocalize with the IMC1 protein on the small concave structures of developing daughter cells. The enrichment of ALP1 on the daughter IMCs continued until their growth was completed, after which ALP1 dispersed back into the cytoplasm as daughter cell budding commenced. The return of ALP1 to the cytoplasm may coincide with the maturation of the IMC1 protein, which relies on a proteolytic processing event at the C terminus that occurs shortly before daughter budding (26). It is hypothesized that the timed cleavage of IMC proteins occurs in order for newly forming parasites to maintain a flexible IMC as they grow within the protective environment of the mother cell but rapidly transform the IMC into a more rigid structure when faced with the outside environment (30).

Immuno-EM also revealed a potential role for ALP1 in the biogenesis of the IMC. ALP1 localized to the IMC at the earliest points in daughter cell formation during the initial formation of the flattened cisternae that associate with the

---

and the presence of daughter IMC1 staining in the latter. (ii) Parasites that maintain ALP1-HA9 overexpression were outcompeted by sibling parasites that downregulated or lost expression. (iii) Some ALP1-HA9-expressing parasites completely failed to initiate daughter cell formation, resulting in nuclear division without cytokinesis (arrow). (iv) Nuclear division continued for several rounds without daughter cell formation (arrow). ALP1-HA9-expressing parasites were detected using a rabbit polyclonal antiserum to HA9 (Zymed, Invitrogen) followed by secondary antibodies conjugated to Alexa 488 (green). IMC1 was detected with mAb 45.15 followed by secondary antibodies conjugated to Alexa 594 (red). Nuclear material was stained with DAPI. Scale bars, 5 μm.

conoid. Immunogold staining was detected on membranes of the nascent daughter cells and on vesicles that bridged the space between the mother nucleus and the daughter. These may be transport vesicles destined for the growing IMC of the daughters. Occasionally, ALP1 staining was also clustered at a discrete region on the leading extension of the dividing nucleus as it was pulled into a daughter (Fig. 6B), suggesting that the ALP1-associated vesicles originate from the ER. Costaining with PDI indicated that these vesicles are likely derived from the ER. Since the protein sequence of ALP1 does not contain a signal peptide, we presume that it associates with the cytoplasmic face of these membranous vesicles as they bud from the nuclear envelope and are delivered to the daughter cells. ALP1 staining was detected on nascent IMC membranes of the daughter cells prior to prominent staining with IMC1 (compare Fig. 7F and G), corroborating the findings by time-lapse microscopy (see the movie in the supplemental material). Collectively, these findings indicate that ALP1 is associated with daughter cell formation at an early time point, likely prior to the delivery of IMC1.

The origin of the cisternae, which make up the inner membrane of the IMC, has not been determined. It was previously suggested that these membranes are Golgi apparatus derived based on early EM studies (39). Others reported previously that the IMC is composed of a specialized ER membrane (7). Our EM data indicate that ALP1 binds to ER-derived vesicles that are destined for the newly forming daughter cells. These vesicles likely traffic through the Golgi apparatus since treatment with brefeldin blocks the elongation of the daughter cell IMC (Gordon, unpublished). The continued association of ALP1 with the IMC membranes as they elongate and accumulate IMC1 protein suggests that ALP1 may function in escorting vesicles or in the scaffolding of the membranes as they are flattened into cisternae of the IMC. There is a precedent for actin being involved in vesicle transport during endocytosis and exocytosis in yeast and mammalian cells (24), and ALP1 may fulfill an analogous function during daughter cell formation. The formation of the IMC from flattened cisternae is unique to the *Apicomplexa*, in keeping with the fact that ALP1 is phylogenetically restricted to this phylum.

We were unable to disrupt the *ALP1* gene by both direct methods and a conditional knockout based on the tetracycline repressor system (27). The inability to obtain a conditional knockout suggests an incompatibility of the regulatable promoters with the cellular function of ALP1, and this is likely due to inappropriate levels or the timing of expression. Consistent with this, the overexpression of ALP1 had a dramatic effect on daughter cell formation. Cell division was blocked such that the average number of parasites per vacuole was greatly decreased and overexpression was rapidly selected against in culture. Moreover, ALP1 overexpression often led to defects in daughter cell IMC formation and errors in nuclear and apicoplast segregation, asymmetric cell division, and reduced growth. The wide range of phenotypes in ALP1 overexpressers is expected from transient expression, where timing or expression differences are likely to occur between different cells in the population. Cells with less severe phenotypes generate daughter cells defined by new IMC structures, yet they tend to divide the nucleus and apicoplast asymmetrically and hence grow less productively. In more severely affected cells, overexpression resulted in the failure to initiate new daughter cells as evidenced by a lack of IMC formation, as detected by IMC1 staining. In such cells, the absence of new daughter cell IMCs did not interfere with nuclear division, and cells with two or even four nuclei were commonly observed, in keeping with previous studies showing that apicomplexans lack normal cell cycle checkpoints associated with cytokinesis (31, 33, 38).

Several previous studies also described perturbations that disrupt daughter cell formation in *Toxoplasma*. For example, the inhibition of microtubule polymerization results in aberrant nuclear division and disruption of daughter cells (31). The overexpression of a GFP fusion of MORN1 also disrupts daughter cell formation (14). However, in both of these cases, large membrane sheets of IMC1 accumulate in the cell, yet they are not able to assemble properly. This phenotype was not observed in ALP1 overexpression, where severely affected cells instead failed to form new daughter cell IMCs, as detected with IMC1 staining. These results imply that ALP1 overexpression does not affect the underlying microtubule scaffold or the stability of the IMC once it begins assembly. Rather, ALP1 overexpression appears to disrupt the initial formation of the IMC. The role of most of the remaining ALPs and Arps has also not been explored in parasites, yet others might participate in cell division, as suggested by the finding that a cosmid containing ARP4 was capable of rescuing a late mitotic phenotype called "multiple nuclear divisions" (13).

Daughter cell formation initiates with the coalescence of a flattened vesicle with singlet microtubules (39). This structure elongates to form the cup-like shape of the conoid, and singlet microtubules grow beneath the forming IMC. The proximity of ALP1 to the early daughter cell conoids and its concentration on membranes in this vicinity (Fig. 7) suggest that it may function in trafficking or the coalescence of these vesicles into the membrane sheets that form the IMC. Overexpression disrupts this process, and cells fail to form daughter cell IMC scaffolds as defined by the IMC1 protein. The block in daughter cell formation caused by the overexpression of ALP1 may result from disrupted vesicle trafficking or from the inability to assemble the membrane plates that make up the IMC. Collectively, our studies suggest that ALP1 participates in the initial stages of daughter cell formation and indicate that further studies of its mechanism may help elucidate how this complex cellular process is governed.

REFERENCES

1. **Bahl, A., B. Brunk, J. Crabtree, M. J. Fraunholz, B. Gajria, G. R. Grant, H. Ginsburg, D. Gupta, J. C. Kissinger, P. Labo, L. Li, M. D. Mailman, A. J. Milgram, D. S. Pearson, D. S. Roos, J. Schug, C. J. Stoeckert, Jr., and P. Whetzel.** 2003. PlasmodB: the Plasmodium genome resource. A database integrating experimental and computational data. Nucleic Acids Res. **31:** 212–215.
2. **Becker, E., N. C. Herrera, F. Q. Gunderson, A. I. Derman, A. L. Dance, J. Sims, R. A. Larsen, and J. Pogliano.** 2006. DNA segregation by the bacterial actin AlfA during *Bacillus subtilis* growth and development. EMBO J. **25:** 5919–5931.

3. **Carballido-Lopez, R.** 2006. The bacterial actin-like cytoskeleton. Microbiol. Mol. Biol. Rev. **70:**888–909.

4. **Cesbron-Delauw, M. F., B. Guy, R. J. Pierce, G. Lenzen, J. Y. Cesbron, H. Charif, P. Lepage, F. Darcy, J. P. Lecocq, and A. Capron.** 1989. Molecular characterization of a 23-kilodalton major antigen secreted by *Toxoplasma gondii*. Proc. Natl. Acad. Sci. USA **86:**7537–7541.

5. **Clark, S. W., and D. I. Meyer.** 1992. Centractin is an actin homologue associated with the centrosome. Nature (London) **359:**246–250.

6. **Delbac, F., A. Sanger, E. M. Neuhaus, R. Stratmann, J. W. Ajioka, C. Toursel, A. Herm-Gotz, S. Tomavo, T. Soldati, and D. Soldati.** 2001. *Toxoplasma gondii* myosins B/C: one gene, two tails, two localizations, and a role in parasite division. J. Cell Biol. **155:**613–623.

7. **de Melo, E. J. T., and W. de Souza.** 1997. A cytochemistry study of the inner membrane complex of the pellicle of tachyzoites of *Toxoplasma gondii*. Parasitol. Res. **83:**252–256.

8. **Dobrowolski, J. M., and L. D. Sibley.** 1996. Toxoplasma invasion of mammalian cells is powered by the actin cytoskeleton of the parasite. Cell **84:**933–939.

9. **Dubey, J. P., D. S. Lindsay, and C. A. Speer.** 1998. Structures of *Toxoplasma gondii* tachyzoites, bradyzoites, and sporozoites and biology and development of tissue cysts. Clin. Microbiol. Rev. **11:**267–299.

10. **Fox, B. A., A. A. Belperron, and D. J. Bzik.** 2001. Negative selection of herpes simplex virus thymidine kinase in *Toxoplasma gondii*. Mol. Biochem. Parasitol. **116:**85–88.

11. **Gilbert, L. K., S. Ravindra, J. M. Turetzky, J. C. Boothroyd, and P. J. Bradley.** 2007. *Toxoplasma gondii* targets a protein phosphatase 2C to the nuclei of infected host cells. Eukaryot. Cell **6:**73–83.

12. **Gordon, J. L., and L. D. Sibley.** 2005. Comparative genome analysis reveals a conserved family of actin-like proteins in apicomplexan parasites. BMC Genomics **6:**179.

13. **Gubbels, M. J., M. Lehmann, M. Muthalgi, M. E. Jerome, C. F. Brooks, T. Szatanek, J. Flynn, B. Parrot, J. Radke, R. Streipen, and M. W. White.** 2008. Forward genetic analysis of the apicomplexan cell division cycle in *Toxoplasma gondii*. PLoS Pathog. **4:**e36.

14. **Gubbels, M. J., S. Vaishnava, N. Boot, J. F. Dubremetz, and B. Striepen.** 2006. A MORN-repeat protein is a dynamic component of the *Toxoplasma gondii* cell division apparatus. J. Cell Sci. **119:**2236–2245.

15. **Gubbels, M. J., M. Weiffer, and B. Striepen.** 2004. Fluorescent protein tagging in *Toxoplasma gondii*: identification of a novel inner membrane complex component conserved among Apicomplexa. Mol. Biochem. Parasiol. **137:**99–110.

16. **Hager, K. M., B. Striepen, L. G. Tilney, and D. S. Roos.** 1999. The nuclear envelope serves as an intermediary between the ER and Golgi complex in the intracellular parasite *Toxoplasma gondii*. J. Cell Sci. **112:**2631–2638.

17. **Harlow, E., and D. Lane.** 1988. Antibodies: a laboratory manual. Cold Spring Harbor Laboratory, Cold Spring Harbor, NY.

18. **Hu, K., T. Mann, B. Striepen, C. J. M. Beckers, D. S. Roos, and J. M. Murray.** 2002. Daughter cell assembly in the protozoan parasite *Toxoplasma gondii*. Mol. Biol. Cell **13:**593–606.

19. **Huttenlauch, I., and R. Stick.** 2003. Occurrence of articulins and epiplasmins in protists. J. Eukaryot. Microbiol. **50:**15–18.

20. **Kato, M., M. Sasaki, S. Mizuno, and M. Harata.** 2001. Novel actin-related proteins in vertebrates: similarities of structure and expression pattern to Arp6 localized on *Drosophila* heterochromatin. Gene **268:**133–140.

21. **Kim, K., M. S. Eaton, W. Schubert, S. Wu, and J. Tang.** 2001. Optimized expression of green fluorescent protein in *Toxoplasma gondii* using thermostable green fluorescent protein mutants. Mol. Biochem. Parasitol. **113:**309–313.

22. **Kim, K., D. Soldati, and J. C. Boothroyd.** 1993. Gene replacement in *Toxoplasma gondii* with chloramphenicol acetyltransferase as selectable marker. Science **262:**911–914.

23. **Kissinger, J. C., B. Gajria, L. Li, I. T. Paulsen, and D. S. Roos.** 2003. ToxoDB: accessing the *Toxoplasma gondii* genome. Nucleic Acids Res. **31:**234–236.

24. **Lanzetti, L.** 2007. Actin in membrane trafficking. Curr. Opin. Cell Biol. **19:**453–458.

25. **Mann, T., and C. Beckers.** 2001. Characterization of the subpellicular network, a filamentous membrane skeletal component in the parasite *Toxoplasma gondii*. Mol. Biochem. Parasitol. **115:**257–268.

26. **Mann, T., E. Gaskins, and C. Beckers.** 2002. Proteolytic processing of TgIMC1 during maturation of the membrane skeleton of *Toxoplasma gondii*. J. Biol. Chem. **277:**41240–41246.

27. **Meissner, M., D. Schluter, and D. Soldati.** 2002. Role of *Toxoplasma gondii* myosin A in powering parasite gliding and host cell invasion. Science **298:**837–840.

28. **Messina, M., I. R. Niesman, C. Mercier, and L. D. Sibley.** 1995. Stable DNA transformation of *Toxoplasma gondii* using phleomycin selection. Gene **165:**213–217.

29. **Morrissette, N. S., J. M. Murray, and D. S. Roos.** 1997. Subpellicular microtubules associate with an intramembranous particle lattice in the protozoan parasite *Toxoplasma gondii*. J. Cell Sci. **110:**35–42.

30. **Morrissette, N. S., and L. D. Sibley.** 2002. Cytoskeleton of apicomplexan parasites. Microbiol. Mol. Biol. Rev. **66:**21–38.

31. **Morrissette, N. S., and L. D. Sibley.** 2002. Disruption of microtubules uncouples budding and nuclear division in *Toxoplasma gondii*. J. Cell Sci. **115:**1017–1025.

32. **Mullins, R. D., J. A. Heuser, and T. D. Pollard.** 1998. The interaction of Arp2/3 complex with actin: nucleation, high affinity pointed end capping, and formation of branching networks of filaments. Proc. Natl. Acad. Sci. USA **95:**6181–6186.

33. **Radke, J. R., B. Striepen, M. N. Guerini, M. E. Jerome, D. S. Roos, and M. W. White.** 2001. Defining the cell cycle for the tachyzoite stage of *Toxoplasma gondii*. Mol. Biochem. Parasitol. **115:**165–175.

34. **Radke, J. R., and M. W. White.** 1998. A cell cycle model for the tachyzoite of *Toxoplasma gondii* using the herpes simplex virus thymidine kinase. Mol. Biochem. Parasitol. **94:**237–247.

35. **Schafer, D. A., and T. A. Schroer.** 1999. Actin-related proteins. Annu. Rev. Cell Dev. Biol. **15:**341–363.

36. **Schroer, T. A., and M. P. Sheetz.** 1991. Two activators of microtubule-based vesicle transport. J. Cell Biol. **115:**1309–1318.

37. **Shaw, M. K., H. L. Compton, D. S. Roos, and L. G. Tilney.** 2000. Microtubules, but not actin filaments, drive daughter cell budding and cell division in *Toxoplasma gondii*. J. Cell Sci. **113:**1241–1254.

38. **Shaw, M. K., D. S. Roos, and L. G. Tilney.** 2001. DNA replication and daughter cell budding are not tightly linked in the protozoan parasite Toxoplasma gondii. Microbes Infect. **3:**351–362.

39. **Sheffield, H. G., and M. L. Melton.** 1968. The fine structure and reproduction of *Toxoplasma gondii*. J. Parasitol. **54:**209–226.

40. **Shen, X., R. Ranallo, E. Choi, and C. Wu.** 2003. Involvement of actin-related proteins in ATP-dependent chromatin remodeling. Mol. Cell **12:**147–155.

41. **Sibley, L. D.** 2004. Invasion strategies of intracellular parasites. Science **304:**248–253.

42. **Soête, M., D. Camus, and J. F. Dubremetz.** 1994. Experimental induction of bradyzoite-specific antigen expression and cyst formation by the RH strain of *Toxoplasma gondii* in vitro. Exp. Parasitol. **78:**361–370.

43. **Soête, M., B. Fortier, D. Camus, and J. F. Dubremetz.** 1993. *Toxoplasma gondii*: kinetics of bradyzoite-tachyzoite interconversion in vitro. Exp. Parasitol. **76:**259–264.

44. **Soldati, D., and J. C. Boothroyd.** 1993. Transient transfection and expression in the obligate intracellular parasite *Toxoplasma gondii*. Science **260:**349–352.

45. **Striepen, B., M. J. Crawford, M. K. Shaw, L. G. Tilney, F. Seeber, and D. S. Roos.** 2000. The plastid of *Toxoplasma gondii* is divided by association with the centrosomes. J. Cell Biol. **151:**1423–1434.

46. **Striepen, B., C. N. Jordan, S. Reiff, and G. G. van Dooren.** 2007. Building the perfect parasite: cell division in Apicomplexa. PLoS Pathog. **3:**691–698.

47. **Striepen, B., D. Soldati, N. Garcia-Reguet, J. F. Dubremetz, and D. S. Roos.** 2001. Targeting of soluble proteins to the rhoptries and micronemes in *Toxoplasma gondii*. Mol. Biochem. Parasitol. **113:**45–53.

48. **Szerlong, H., A. Saha, and B. R. Cairns.** 2003. The nuclear actin-related proteins Arp7 and Arp9: a dimeric module that cooperates with architectural proteins for chromatin remodeling. EMBO J. **22:**3175–3187.

49. **Vaishnava, S., D. P. Morrison, R. Y. Gaji, J. M. Murray, R. Entzeroth, and D. K. Howe.** 2005. Plastid segregation and cell division in the apicomplexan parasite *Sarcocystis neurona*. J. Cell Sci. **118:**3397–3407.

50. **Weiss, L. M., D. LaPlace, H. B. Tanowitz, and M. Wittner.** 1992. Identification of *Toxoplasma gondii* bradyzoite-specific monoclonal antibodies. J. Infect. Dis. **166:**213–215.